New Techniques to Measure Cliff Change from Historical Oblique Aerial Photographs and Structure-from-Motion Photogrammetry

Authors: Warrick, Jonathan A., Ritchie, Andrew C., Adelman, Gabrielle, Adelman, Kenneth, and Limber, Patrick W.

New Techniques to Measure Cliff Change from Historical Oblique Aerial Photographs and Structure-from-Motion Photogrammetry

Jonathan A. Warrick[†]*, **Andrew C. Ritchie**[‡], **Gabrielle Adelman**[§], **Kenneth Adelman**[§], **and Patrick W. Limber**[†]

[†]U.S. Geological Survey
Santa Cruz, CA 95060, U.S.A.

[‡]Olympic National Park
Port Angeles, WA 98362, U.S.A.

[§]California Coastal Records Project
Corralitos, CA 95076, U.S.A.

www.cerf-jcr.org

ABSTRACT

www.JCRonline.org

Warrick, J.A.; Ritchie, A.C.; Adelman, G.; Adelman, K., and Limber, P.W., 2017. New techniques to measure cliff change from historical oblique aerial photographs and Structure-from-Motion photogrammetry. *Journal of Coastal Research,* 33(1), 39–55. Coconut Creek (Florida), ISSN 0749-0208.

Oblique aerial photograph surveys are commonly used to document coastal landscapes. Here it is shown that adequate overlap may exist in these photographic records to develop topographic models with Structure-from-Motion (SfM) photogrammetric techniques. Using photographs of Fort Funston, California, from the California Coastal Records Project, imagery were combined with ground control points in a four-dimensional analysis that produced topographic point clouds of the study area's cliffs for 5 years spanning 2002 to 2010. Uncertainty was assessed by comparing point clouds with airborne LIDAR data, and these uncertainties were related to the number and spatial distribution of ground control points used in the SfM analyses. With six or more ground control points, the root mean squared errors between the SfM and LIDAR data were less than 0.30 m (minimum = 0.18 m), and the mean systematic error was less than 0.10 m. The SfM results had several benefits over traditional airborne LIDAR in that they included point coverage on vertical-to-overhanging sections of the cliff and resulted in 10–100 times greater point densities. Time series of the SfM results revealed topographic changes, including landslides, rock falls, and the erosion of landslide talus along the Fort Funston beach. Thus, it was concluded that SfM photogrammetric techniques with historical oblique photographs allow for the extraction of useful quantitative information for mapping coastal topography and measuring coastal change. The new techniques presented here are likely applicable to many photograph collections and problems in the earth sciences.

ADDITIONAL INDEX WORDS: *California Coastal Records Project, photogrammetry, Fort Funston, cliff erosion.*

INTRODUCTION

Measurements of coastal change are essential for calculating trends in erosion or accretion and for evaluating the physical processes that modify coastal landscapes (Bird, 1985; Crowell, Leatherman, and Buckley, 1991; Moore, 2000; Ruggiero *et al.*, 2001; Thieler and Danforth, 1994). Coastal change measurements are also useful as a basis to understand and to predict the response of coastal landforms to storms, climate, and sea-level change that will occur in the future (Cazenave and Cozannet, 2014; Cowell and Kench, 2001; Fitzgerald *et al.*, 2008; Hapke and Plant, 2010; McGranahan, Balk, and Anderson, 2007). Several techniques are used to measure beach and sea-cliff changes, including topographic and bathymetric surveying (Larson and Kraus, 1994; Morton, Paine, and Gibeaut, 1994; Ruggiero *et al.*, 2005), aerial or satellite-based imagery (Fletcher *et al.*, 2003; Hapke and Richmond, 2000; White and El Asmar, 1999), light detection and ranging (LIDAR) from airborne or terrestrial platforms (Rosser *et al.*, 2013; Sallenger *et al.*, 2002; Stockton *et al.*, 2002; Vann Jones *et al.*, 2015; Young et al., 2010), and combinations of these techniques (Adams and Chandler, 2002; Ruggiero *et al.*, 2013; Smith and Zarillo, 1990).

New digital photogrammetry techniques, termed Structure-from-Motion (SfM), have reinvigorated the use of photography from land-based and/or airborne platforms to measure landscape topography and change (Fonstad *et al.*, 2013; James and Robson, 2012; Javernick, Brasington, and Caruso, 2014; Johnson *et al.*, 2014; Snavely, Seitz, and Szeliski, 2006; Westoby *et al.*, 2012). Most applications of SfM include photographic and ground control surveys to build three-dimensional point clouds or two-dimensional height fields (*i.e.* digital elevation models). Repeated collections at a site allow for analyses of change through differencing in the vertical or land-surface normal directions (Eltner *et al.*, 2015; Lague, Brodu, and Leroux, 2013; Prosdocimi *et al.*, 2015; Randle *et al.*, 2015). Testing and assessment of SfM techniques have led to recommendations, such as camera sensor types, optimal camera settings, degree of overlapping images, and inclusion of back-sighted or multiperspective imagery, to limit errors and maximize ground coverage (Agisoft, 2014; James and Robson, 2014; Micheletti, Chandler, and Lane, 2015).

The focus of most SfM applications has been the collection and analysis of new photographs. This, perhaps, is not unusual because SfM requires photographic overlaps across the entire area of interest—and preferably three or more views of each ground point from different camera perspectives—and these requirements are best met with the collection of new imagery. Although new collections allow the user to determine photograph spacing and orientation, historic photographs may exist
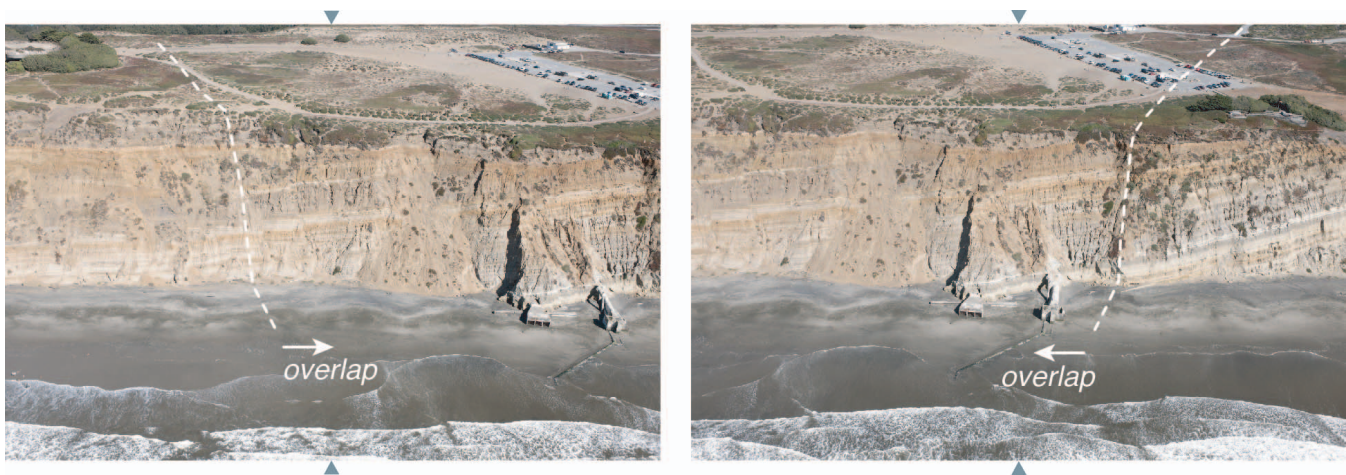
Figure 1. Examples of oblique, aerial photographs of Fort Funston, California, from CCRP (2016). Dashed lines show the approximate overlap between the photos, and photo midpoints are shown with triangles. (Color for this figure is available in the online version of this paper.)

that fulfill the photo overlap requirements, and these kinds of historical photographs may greatly expand the application of SfM (Derrien *et al.*, 2015; Gomez, Hayakawa, and Obanawa, 2015).

Oblique aerial photographic surveys of coastal landscapes are commonly conducted to qualitatively track changes over time or to characterize the impacts of events such as storms (*e.g.,* California Coastal Records Project [CCRP], 2016; Morgan and Krohn, 2014). The amount of photographic overlap in these surveys can vary from greater than 50%, and thus are potentially usable for SfM, to less than 50%, and are generally unusable for SfM (Figure 1). Oblique photographs may be ideal for mapping cliffs owing to the potential to generate topographic data on vertical-to-overhanging sections of cliffs that are traditionally poorly resolved with near-vertical aerial photographs and airborne LIDAR data (Gienko and Terry, 2014; Ružić *et al.*, 2014).

Here the utility of SfM methods to quantitatively map landscape topography from historical, oblique aerial photographs was examined. The primary goal was to evaluate whether these historical photos could be used with additional ground control information to produce accurate topographic maps and topographic change analyses of coastal cliffs through time. Five photographic surveys between 2002 and 2010 from the CCRP (2016) were used to evaluate these goals, and detailed descriptions of optimal techniques and results are provided.

Study Area
The Fort Funston region of central California (Figures 1 and 2) was chosen as the study area owing to its high cliffs that fail intermittently and the regular photographic surveys of this site available in the CCRP. The mean erosion rates of these cliffs have ranged between 0.5 and 1.3 m/y over a 70-year interval, and the rates of erosion are 2–4 times greater than found along the broader region of the central coast of California ($\sim$0.3 m/y; Hapke and Reid, 2007).

The cliffs at Fort Funston expose Pleistocene sedimentary rocks of the Merced formation, which include shallow marine and nonmarine aeolian deposits (Clifton and Hunter, 1999). The deposits are directly adjacent to the San Andreas Fault and have been progressively uplifted (Ryan, Parsons, and Sliter, 2008) and exposed to wave erosion, forming tall, semi-consolidated cliffs that exceed 50 m in height. Because of the high proportion of coarse sediment in these geologic units, the erosion of these cliffs provides littoral-grade sand and gravel to the greater Ocean Beach littoral cell (Limber, Patsch, and Griggs, 2008).

The study area was focused on the tallest section of the Fort Funston cliffs within the Golden Gate National Recreation Area (Figure 2c). Extending from a beach access trail in the north to the termination of the tall cliffs immediately south of the park's main parking lot, this study area incorporated 0.88 km of sea cliffs (Figure 2c). As part of the Golden Gate National Recreation Area, the study area is managed as open space with limited development. Numerous historical structures exist throughout the site, and most of these were military defense installations built during the early- to mid-20th century. Although these structures provide stable features for ground control points, evidence also exists in the CCRP (2016) photos that some of these structures have moved with time because of the eroding cliffs and littoral processes.

METHODS
Topographic point clouds for the Fort Funston study area were generated with SfM algorithms, oblique aerial photographs and their metadata, and survey-grade ground control points and positions within the study area.

Data
Several sources of data were utilized to develop and analyze the SfM results. The primary source data were photographs from CCRP (2016). Ground control was provided with survey-grade topographic positions of stable points that were easily
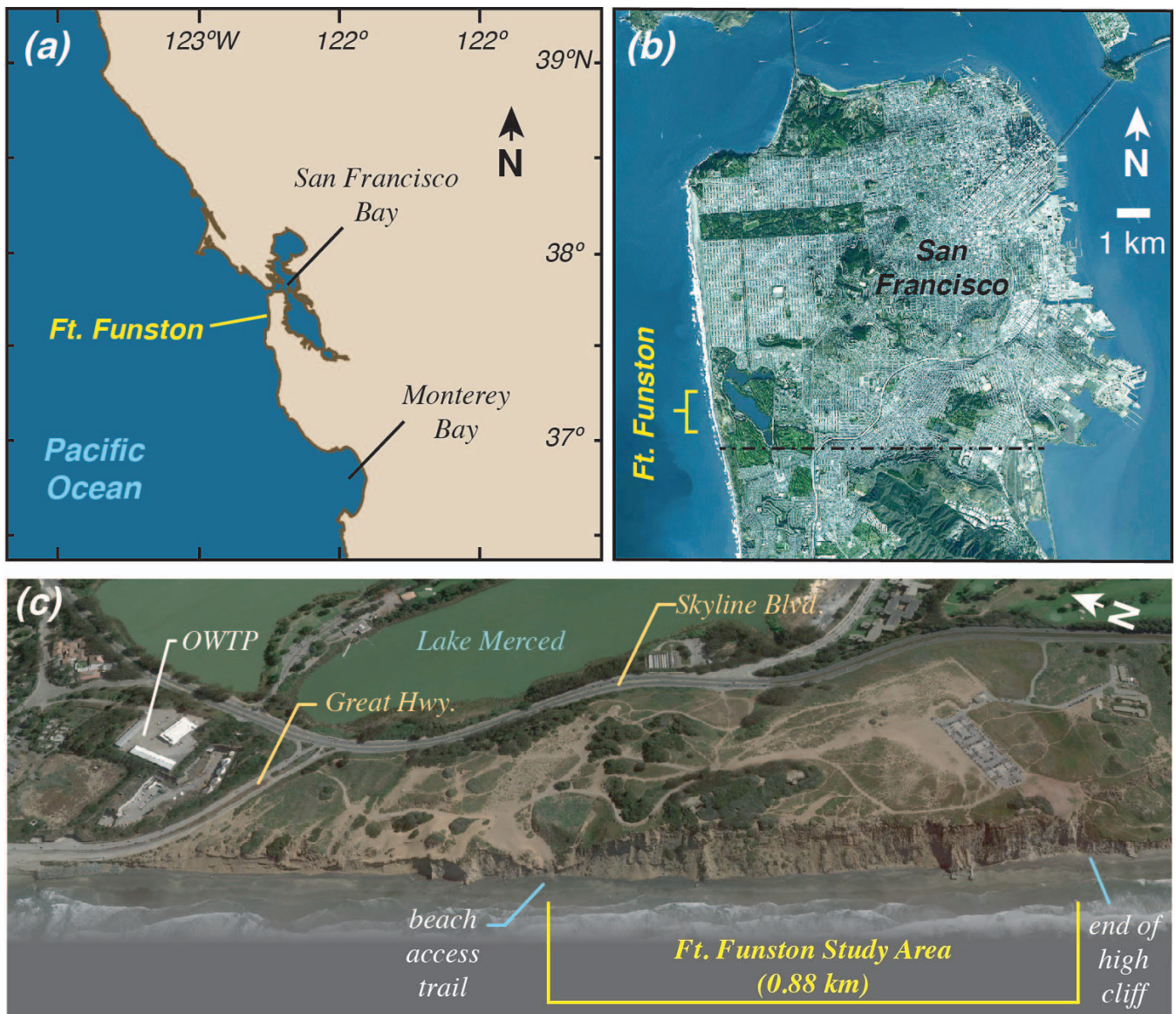
Figure 2. Maps of the Fort Funston, California, study area, including (a) regional perspective and (b) local maps. (c) Oblique shaded-relief map of the Fort Funston study area showing the 0.88-km length of study area between the beach access trail in the north and the end of the high cliff in the south. Also shown is the Oceanside Wastewater Treatment Plant (OWTP). Imagery from Google Earth (2016). (Color for this figure is available in the online version of this paper.)

identifiable in the imagery and in the field. Finally, airborne LIDAR data were used to evaluate the uncertainty in the SfM-derived point clouds.

Oblique Photographs

The CCRP was established to photographically document baseline conditions of the California coast and to monitor changes with time (CCRP, 2016). Photographs have been taken with a handheld digital single-lens reflex camera from a helicopter flying at approximately 150–200 m elevation for the Fort Funston study area and 50–600 m elevation across the broader state of California. Photographic surveys have been conducted regularly in the late summer to early fall since 2002.

Several camera models have been used throughout the project, and the quality and resolution of the photos have generally improved with each new camera system (CCRP, 2016; Table 1). Cameras have been fitted with a 28–70-mm zoom lens, which allows for manual setting of the field-of-view to the coastal region of interest. Photographs have been taken at oblique angles, and they generally capture an area from the inner surfzone to the tops of the coastal cliffs or inland portions of the coastal landscape (e.g., Figure 1). The Fort Funston region was consistently flown from north to south.

Although originally saved in the Nikon raw format (.NEF), images have been transformed into JPEG-formats and archived by geographic location and survey date on the project's

Table 1. *Summary of the aerial photographs used to map the Fort Funston cliffs.*

Survey Year	Date of Flight	Number of Photos	Photo IDs	Camera Type	Photo Resolution	Lens Settings
2002	30 September 2002	11[a]	5814 to 5825[a]	Nikon D1x	3008 × 1960	28 mm (1); 35mm (5); 38 mm (3); 42 mm (2)
2004	21 September 2004	9	200400406 to 200400414	Nikon D1x	3008 × 1960	38 mm (9)
2008	1 October 2008	14	200809257 to 200809270	Nikon D2x	4296 × 2860	45 mm (8); 48 mm (5); 50 mm (1)
2009	1 October 2009	15	200906500 to 200906514	Nikon D3x	6064 × 4036	38 mm (2); 40 mm (13)
2010	25 September 2010	13	201007783 to 201007795	Nikon D3x	6064 × 4036	48 mm (13)

[a] One photo (ID 5819) was obtained of a small aircraft in flight immediately above the cliff face. This highly zoomed photograph (70 mm) captured little of the cliff face and was excluded from the analyses.

website (CCRP, 2016). To mimic the future use of these archived photos by others, the archived JPEG imagery were used in the analyses here. Additionally, metadata have been incorporated into each photograph's EXIF data, and several of these are useful for the SfM analyses. These include the photograph settings from the camera (including the manually set lens focal length) and the location and time information of the photo obtained from a Garmin GPS-35 that was mounted to the helicopter, sampled at 1 Hz, and electronically connected to the camera. Position accuracy for each photo was estimated using a helicopter speed of ∼60 m/s and a GPS-camera delay of up to 0.1 second, which results in a worst-case travel distance between the previous GPS update and the photo of 66 m. Combined with the GPS positional accuracy of 5–10 m, the mean uncertainty of the photo positions was at least tens of meters, with a systematic along-track bias owing to the delays between the GPS and photo acquisition times.

All photos were obtained from the CCRP (2016) website at the highest resolution available (Table 1). For each survey year, photos were obtained for the entire 0.88-km study area with an additional photo on both ends to ensure the mapping products fully covered the study area. To best compare the SfM results with the 1998 and 2010 LIDAR, all photo records through the year 2010 were used. During early trial and error analyses, one available survey year (2005) was found to have inadequate overlap between the photos and was not included in the analyses here. Thus, five photographic surveys were included, and between 9 and 15 images were included per survey (Table 1).

Ground Control Points

On 3 February 2015, a survey was conducted to measure survey-grade geographical coordinates of hard structures and features in the Fort Funston study area for the purpose of ground control for the SfM analyses. Although over 100 points were measured throughout Fort Funston, only 41 of these points were determined to be easily observable in the survey photos and on features that had not moved during 2002 to 2015. Evidence for movement was provided in the series of CCRP (2016) photos. Ground control points were surveyed with a Trimble R7 differential GPS (DGPS) with an antenna mounted on a 2-m survey rod. Each point was occupied for 10 seconds, and DGPS corrections were provided by a GPS station operated by the U.S. Geological Survey (USGS) and mounted at the Oceanside Waste Treatment Plant, San Francisco (*cf.* Barnard, Hansen, and Erikson, 2012; Figure 2). All position data were output in the projected coordinate system, NAD83 UTM 10N with a NAVD88 vertical datum. Because the maximum baseline distance was 1.5 km and potential for minor user

sampling errors exists, the horizontal and vertical uncertainties in ground control point positions were less than 5 cm (*cf.* Barnard, Hansen, and Erikson, 2012). Further details and position data for the ground control points are provided in the Supplemental Materials section.

Airborne LIDAR

Two airborne LIDAR surveys were available and were used to compare the SfM-generated data. The LIDAR survey data were obtained, with metadata, from the publically accessible NOAA Digital Coast website (2016). Flights occurred at or near low tide and extended only a few km inland from the coast. The 1998 dataset was collected after the 1997–98 El Niño winter season using NASA's Airborne Topographic Mapper with a single-return green laser. Because the data were unclassified, they include returns from vegetation and the water surface. Vertical and horizontal accuracy is reported to be 15 cm and 80 cm, respectively, with a nominal point spacing of 3 m.

The 2010 dataset was collected using an Optech ALTM 3100EA LIDAR system and included four discrete return types (unclassified, ground, noise, and water surface). To be consistent with the 1998 LIDAR survey and the point clouds generated by SfM that lack penetration of vegetation, only the unclassified LIDAR returns from 2010 were used. Vertical and horizontal accuracy of the 2010 dataset were reported to be 12 cm and 200 cm, respectively, with a nominal point spacing of 0.7 m; however, for both LIDAR data sets the point spacing increased significantly on steep-to-overhanging slopes because lasers were shot at near vertical orientations.

For comparisons with the SfM results, the LIDAR data were clipped spatially to areas of the cliff face, talus at the base of the slope, and the unvegetated cliff top. This was done by removing all LIDAR returns within tree canopies and on the sandy beach using clipping tools in the Cloud Compare software, version 2.6.1 (2016).

SfM Analyses

All of the SfM analyses were conducted with the commercially available Agisoft PhotoScan Pro software (version 1.1.6; 2016). The goal of the SfM analyses was to produce high-resolution, accurate, and precise topographic point clouds.

Photo Alignment and Camera Calibration

The first step in building SfM-derived topographic point clouds focused on solving the alignment parameters of the photographs (*i.e.* the geographic positions and orientations) and the camera calibration parameters. Although this step is commonly conducted using a collection of photographs from a single survey, it was found that single collections of the CCRP
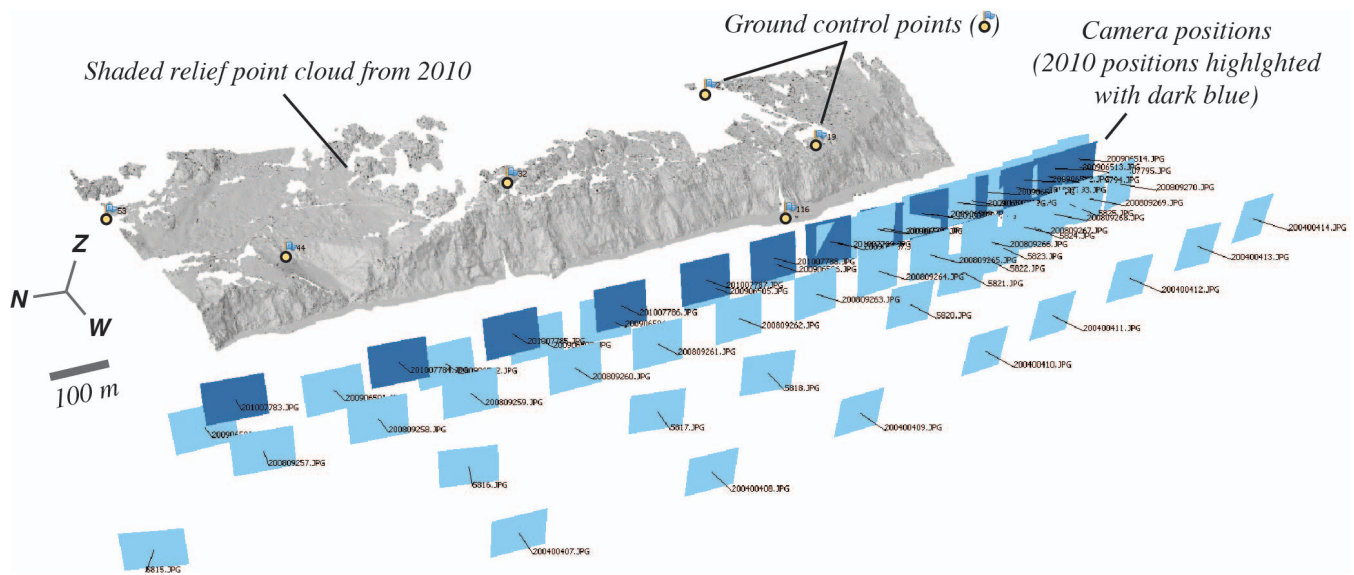
Figure 3. Oblique presentation of the four-dimensional (4D) Structure-from-Motion (SfM) analysis of the Fort Funston study area. The image includes a shaded-relief map of surface point cloud computed from the 2010 imagery (grey shading), camera positions and orientations from all five photographic surveys (blue symbols with black lines), the camera positions for the 2010 survey highlighted (darker blue symbols), and 6 of the 41 ground control points (flagged yellow symbols). (Color for this figure is available in the online version of this paper.)

(2016) photographs resulted in incomplete and/or poorly aligned point clouds, largely owing to limitations in photo overlap (not all pairs of sequential photos had >50% overlap). Additionally, along-track systematic errors can often occur in a series of photos taken in a straight line (*cf.* James and Robson, 2014).

Thus, four-dimensional (4D) techniques were used to align photos and to calibrate the camera optics. To accomplish this, all photos from all photographic survey dates were incorporated into a photo alignment and camera calibration process (Figure 3). A 4D technique can benefit from multiple views of stationary objects with time as long as the objects are resolved at about the same photographic scales and as long as they remain stationary. Applying this technique to all 62 photos from the 5 years of collections resulted in 6–12 independent views of every ground location within the study area and much better final alignment, as measured by the error assessments described below.

The alignment process included several preprocessing steps. First, to provide an initial estimate of the geographical positions of each photo, the photo GPS locations were converted into the projected coordinate system, NAD83 UTM10N, from the WGS data stored in the photo EXIF. Then, masks were made to eliminate portions of each photo that would not beneficially contribute to alignment calculations owing to physical motion (such as found in the surfzone) or owing to broad, uniform color patterns (such as found in the sky). For consistency, all surfzone swash and sky pixels, where present, were masked from the photos. The swash zone was masked up to the limits of the observable wet-dry line. Other minor objects that may have been in motion, including people, birds, and cars, were not masked from the analyses.

Camera calibration groups were then organized to ensure optimal calculation of camera calibration parameters. Calibration parameters are computed by the PhotoScan software (Agisoft PhotoScan Pro software, 2016) for each calibration

Table 2. *Summary of the SfM-derived topographic point clouds and the available LIDAR for the Fort Funston study area.*

Survey Year	Average Number of Tie Points Per Photo	Number of Topographic Points Generated (Millions pt)	Mean Point Density on Cliff Face (pts/m^2)[a]	File Size, Photoscan Project[b] (Mb)	File Size, .LAS (Mb)
2002	981	3.50	26	28.9	88.8
2004	1285	2.67	17	24.1	67.7
2008	1473	14.34[c]	111[c]	93.5	364.0[c]
2009	1079	21.80[c]	123[c]	141.4	553.6[c]
2010	1423	22.90[c]	161[c]	148.5	581.4[c]
1998 LIDAR	NA	0.20	0.6	–	6.7
2010 LIDAR	NA	0.50	2.0	–	16.6

[a] Computed on areas parallel to the cliff face.

[b] Agisoft PhotoScan Pro software (2016).

[c] Point clouds with greater than 10 million points were randomly subsampled to 10 million for all analyses shown in this paper. This resulted in mean point densities of 78, 56, and 70 per m^2 for 2008, 2009, and 2010, respectively, and .Las file sizes that were 332.0 Mb.
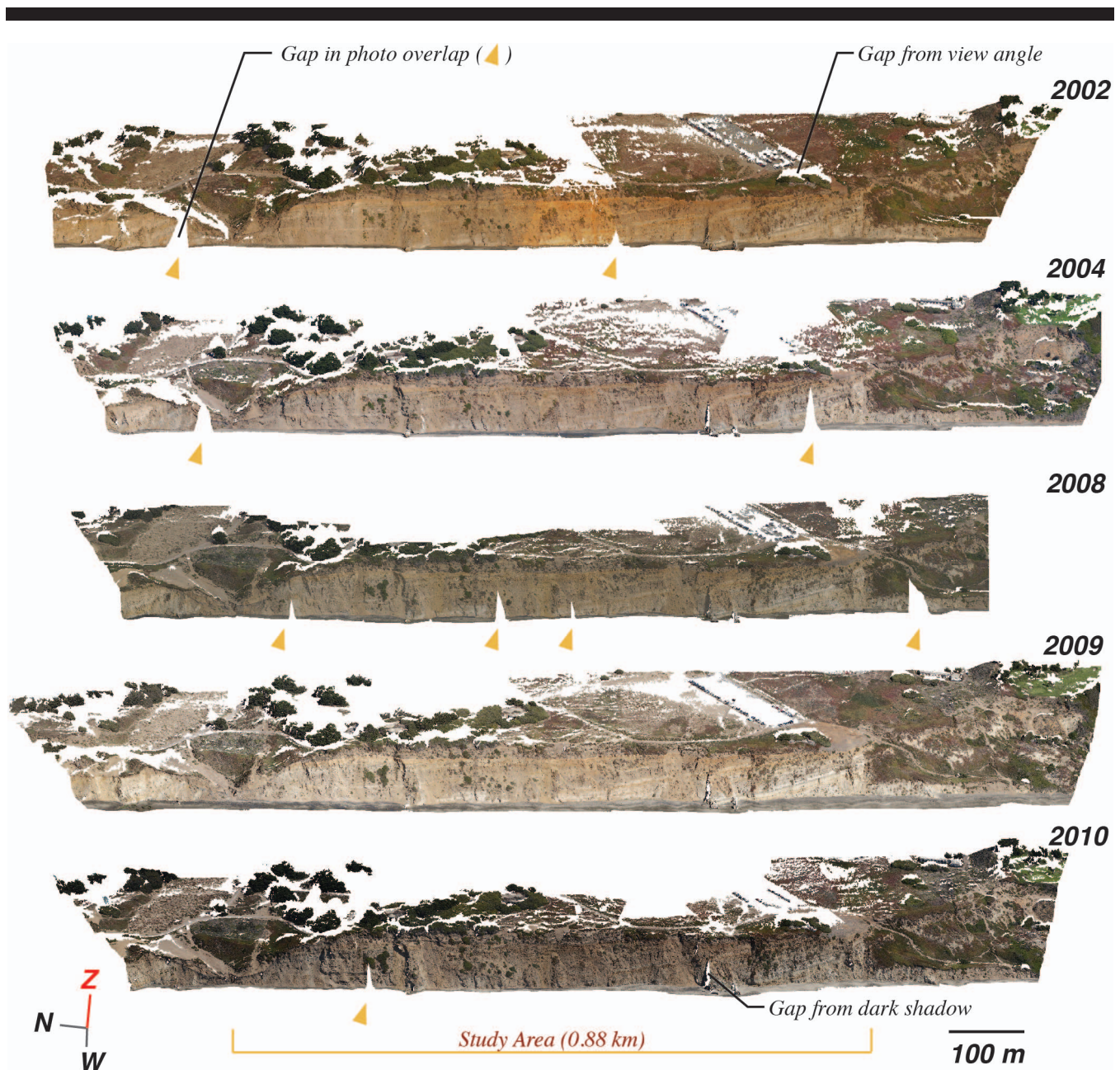
Figure 4. Three-dimensional point clouds generated for the Fort Funston study area using SfM and 5 years of oblique historical photos. Gaps in the point clouds were caused by either gaps in photo overlaps (yellow arrows), ground areas unseen in the imagery owing to view angle, or areas masked by dark shadows.

group by minimizing errors during the alignment and calibration steps; these calibration groups were initially assigned using camera type and lens focal length data stored in the photo EXIF data. For the purposes of this analysis, however, it was assumed that lens focal lengths were truly constant (*i.e.* unaltered by the photographer) only during successions of photos with equivalent focal lengths. If photos had identical camera settings but were not in succession, then they were separated into different camera calibration groups,

owing to the impracticality of returning a zoom lens back to an identical focal length.

After these preprocessing steps, initial solutions to the photo alignments and camera calibrations were generated using the Align Photos tool in the PhotoScan software (Agisoft PhotoScan Pro software, 2016). During this process, unique points in each photo, termed key points, were identified and tied (or matched) across the body of photos. These resulting tie points become the basis for determining camera and scene geometries using
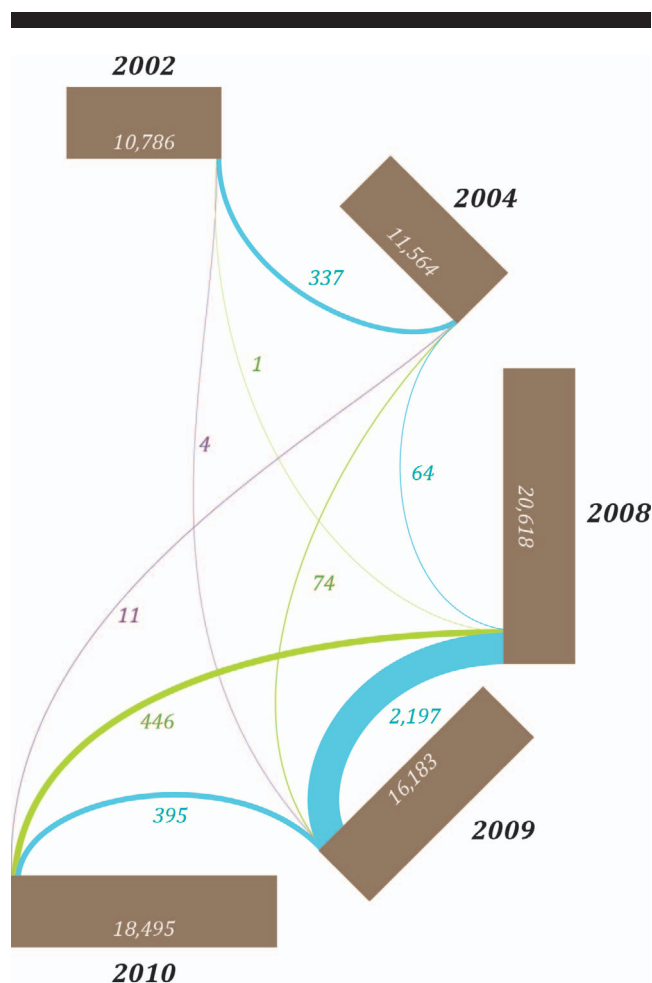
Figure 5. Relationships of the shared tie points across photo survey years from the 4D analyses. The brown bars are scaled and labeled with the total number of unique tie points within each survey. Lines connecting these bars are scaled and labeled with the number of shared tie points between the two survey years. (Color for this figure is available in the online version of this paper.)

photogrammetric principles and minimizing errors in the solutions to solved parameters. Several options were available for this photo-alignment step, but the overarching goals were to produce approximately several thousand tie points per image, to have the tie points well distributed within and throughout the photos, and to exclude false or poorly resolved ties.

These goals were achieved by modifying the standard settings and processing steps in several ways. First, the total limit of tie points and key points were allowed to be 4000 and 40,000 per image, respectively. Larger values for these settings generally increased the abundance of false ties and increased the root mean squared error (RMSE) of the tie point positions. Using these settings and the highest computational accuracy setting for the analysis resulted in 152,733 well-distributed tie points for the Fort Funston photos, and the number of points in each photo ranged between 614 and 5263. Many of the tie points crossed between survey years, providing spatial links necessary for the 4D analyses.

Inaccurate and poorly resolved tie points were then removed using a several step technique (Thomas Noble, U.S. Bureau of Land Management, *personal communication*). First, points that were positioned well above, below, or beyond the landscape were removed with an editing tool. A total of 242 tie points, or 0.16%, were removed in this manner. Then, several tie-point metrics were used to identify and remove points with poorly resolved solutions. Tie points were removed that had high reconstruction uncertainties, a nondimensional parameter related to directional uncertainties in the point position, and high reprojection errors, a computed metric of the local accuracy of each tie point in pixels (*cf*. Agisoft, 2014). Although some recommended strategies suggest removing all points with greater than 10 reconstruction uncertainty and 0.3-pixel reprojection error (Thomas Noble, U.S. Bureau of Land Management, *personal communication*), it was found that these thresholds removed too many points and thereby resulted in poorly resolved final point clouds. Through iterations, it was concluded that thresholds roughly three times these values resulted in optimal results for the study area. Using a reconstruction uncertainty of greater or equal to 30, a total of 8737 (or ~5.7%) of the tie points were selected and removed. Then, using a reprojection error of greater than or equal to 1.0 pixels, 5507 points (or ~3.6%) were selected and removed.

A first iteration to recalculate optimal camera-calibration parameters was then conducted from the remaining tie points by using the Camera Calibration tool in the Photoscan software, which was solved for the following camera-lens parameters: the focal length (f), the optical center of the photos (cx, cy), the radial distortion factors ($k1$, $k2$, $k3$), the tangential distortion factors ($p1$, $p2$), pixel-aspect ratio (*aspect*), and pixel skew (*skew*; Agisoft, 2014). Because the tie point locations were also recomputed by the PhotoScan software (Agisoft PhotoScan Pro software, 2016) during this step, an additional 402 tie points resulted with uncertainty and error values greater than the thresholds of 30 and 1 pixel. Thus, a second iteration was conducted by removing these points and resolving for the camera-lens parameters. Mean error in the camera positions (compared to the original helicopter GPS) was reported to be 26.76 m, and RMSE of the tie-point cloud was 0.398 pixels. A total of 137,845 tie points remained, and the number of tie points in each photo ranged from 505 to 5092. Averaged for each photographic survey year, the number of tie points ranged between 981 and 1473 per photo (Table 2).

Applying Ground Control

Following the alignment step, ground control points were added to the SfM analyses to improve the camera calibrations and to register the point clouds to geographical coordinates. An evaluation was made about optimal number and spatial distributions of ground control points by independently introducing 3, 4, 6, 8, 10, 12, 15, 20, 25, 30, and 41 of the points to the analyses (11 runs in total; see Supplemental Materials for details). In choosing these points, the most easily identifiable and broadest spatial distribution of points were chosen (*cf*. Figure 3). Because many coastal settings will have opportunities for ground control points only at the top of the cliff and not along the beach, an evaluation was made as to whether the results were influenced by excluding ground
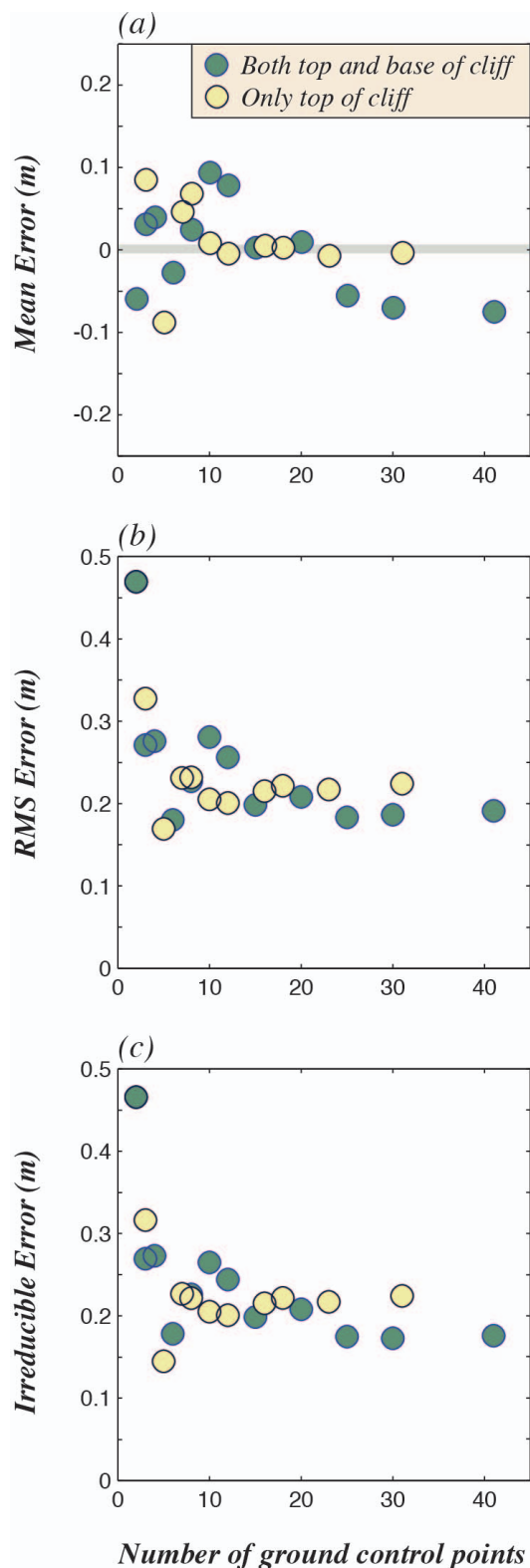
Figure 6. Differences between the 2010 point clouds developed for the Fort Funston study area from SfM and airborne LIDAR, highlighting the effects of the number of ground control points. Errors were computed over the entire study area and include (a) the mean error, (b) the root mean squared error

control points found near the base of the cliff. For these top of the cliff runs, all 11 models were rerun without any of the ground control at the base of the cliff. The top of the cliff runs included between 3 and 31 total ground control points. For all of these runs, a dense SfM topographic point cloud was generated for the 2010 photographic survey to compare with the 2010 airborne LIDAR.

After the appropriate number of ground control points were added to the PhotoScan project, the camera-calibration parameters were optimized one final time using uncertainty settings to match the data (30-m camera positions, 0.05-m marker positions, and 1-pixel tie-point positions) and the camera parameters listed previously. The resulting tie-point clouds were used for generating dense topographic point clouds, as subsequently described.

Generating Topographic Point Clouds

Topographic point clouds were generated for each of the five survey dates with Agisoft PhotoScan software. As subsequently noted, the primary change analyses were developed from point clouds generated with only six ground control points, although point clouds were generated from all configurations of ground control for the purposes of error analyses. For all runs, a bounding box was used to limit the geographical extent of the final product to the areas seaward of Skyline Boulevard (*cf.* Figure 2). Dense topographic point clouds were then generated for the desired survey date by including only photos from the survey using the enable and disable tools provided by the software (Agisoft, 2014). Point clouds were generated using the Build Dense Cloud tool at high resolution with mild depth filtering in the PhotoScan project. These settings resulted in cm-to-dm point cloud densities for the study area and the most limited filtering of outlier points available by the software. The final point clouds included several million to tens of million topographic points, and each point included 8-bit red, green, and blue (RGB) color values sampled from the original photos (Table 2).

The point clouds were exported from PhotoScan (Agisoft PhotoScan Pro software, 2016) using the .LAS standard file format for LIDAR data for the purpose of computations and comparisons. Because the 2008, 2009, and 2010 point clouds contained tens of millions of points, the .LAS files were hundreds of megabytes (Table 2), which hindered computational speeds in subsequent analyses. Thus, the point clouds from these three surveys were subsampled to 10 million points using a random point-selection algorithm in the Cloud Compare software, version 2.6.1 (2016) (Table 2). This resulted in point densities that were 56 to 78 points/m^2 and file sizes that were 332 megabytes.

Analyses of Change

Change analyses between all topographic point clouds were conducted with the Multiscale Model to Model Cloud Comparison (M3C2) techniques of Lague, Brodu, and Leroux (2013)

(RMSE), and (c) the irreducible error. Results shown for ground control points selected from both the top and base of the cliff (dark symbols) and from only the top of the cliff (light symbols). (Color for this figure is available in the online version of this paper.)

(a) Number of ground control points = 3

Ground control points ( )

(b) Number of ground control points = 6

(c) Number of ground control points = 25

Study Area (0.88 km)

Difference between SfM and lidar (m)

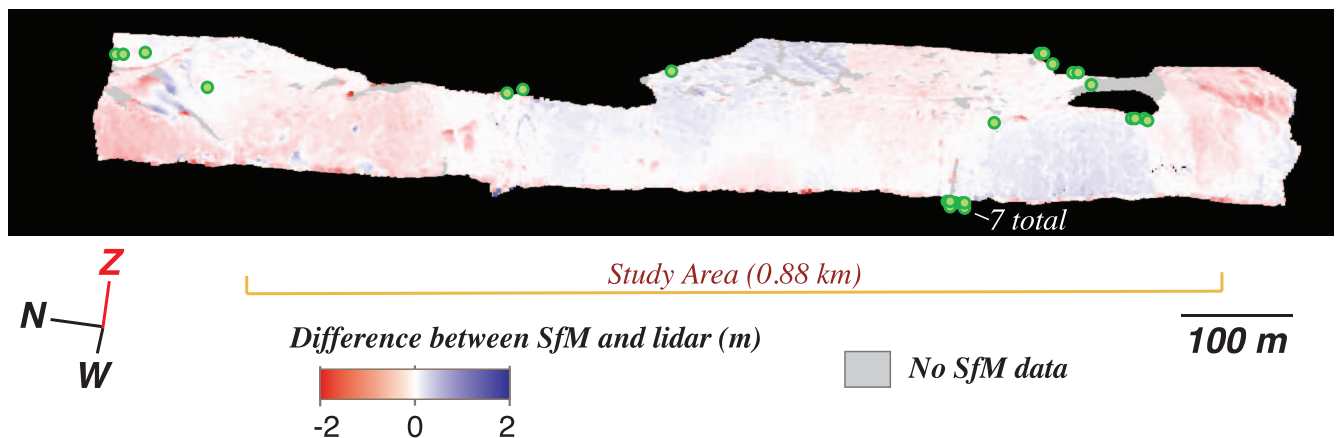*No SfM data*

100 m

-2   0   2

Figure 7. Difference maps between the SfM-derived point clouds and airborne LIDAR for the Fort Funston study area during 2010 to highlight the effects of the number and distribution of ground control points. Three examples are shown: (a) 3, (b) 6, and (c) 25 ground control points. Differences are presented in the direction normal to the SfM-generated surface using the M3C2 methods of Lague, Brodu, and Leroux (2013). Measurements on the trees and beach were removed to eliminate the bias these observations added. Maps are shown from oblique perspectives.

carried out in the Cloud Compare software, version 2.6.1 (2016). The M3C2 technique provides measurements of distance between two point clouds along the direction of local normals from the original ground surface. Several computational parameters are needed for the M3C2 technique to define the nominal spacing between change measurements, the spherical size of influence for computing normal directions, and the area to consider when projecting from one model to the other. In general, these parameters should function with the data density of the original point clouds, and an optimization routine is provided in the M3C2 tool to balance point density and distance measurement accuracy for the available data (*cf.* Lague, Brodu, and Leroux, 2013).

For change assessments between the SfM point clouds, the M3C2 calculations were conducted uniformly at 0.5-m nominal spacing with normal directions and projections calculated at 1.0 m diameters about each point. For the LIDAR-to-LIDAR and LIDAR-to-SfM change assessments, the M3C2-recommended parameters for LIDAR-to-LIDAR were coarser owing to the lower data density in the LIDAR products. Using the M3C2 optimization routine, the recommended parameters were found to be a nominal spacing of 2.7 m and normal directions and projections of 5.4 m about each point.

RESULTS

Topographic point clouds were developed for the 5 years of photographs, and each photographic survey resulted in millions of points across the study-area cliff face (Figure 4; Table 2). Data densities along the cliff face ranged between 17 and 161 points/m^2 and were highest during the most recent
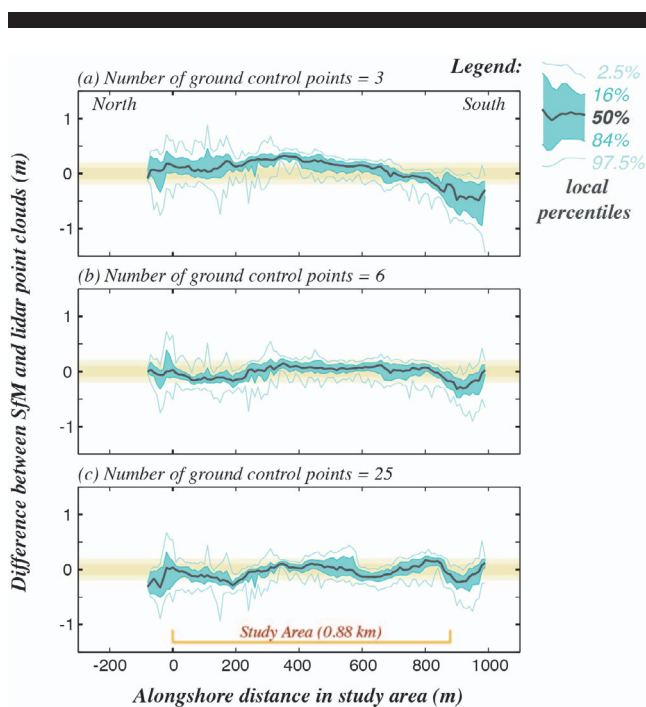
Figure 8. Summary of the alongshore differences between the SfM-derived point clouds and airborne LIDAR along the Fort Funston study area during 2010 for the same examples shown in Figure 7. Data are presented as percentiles of all difference measurements within 10-m alongshore increments. Measurements on the trees and beach were removed to eliminate the bias these observations added. Results shown for (a) 3, (b) 6, and (c) 25 ground control points. The area of ±0.2 m is highlighted with solid yellow. (Color for this figure is available in the online version of this paper.)

surveys owing to increased photographic resolution (Tables 1 and 2); however, gaps were observed in the point clouds in areas without photographic overlap, surfaces not seen from the photo view angles, and regions with dark shadows (Figure 4). The locations of the gaps from view angles and dark shadows were fairly consistent each year because of the relatively consistent flight pathways and timing of the surveys (*cf.* Figure 3; Table 1).

Examination of the tie points that formed the foundation of photo alignment and camera calibration, and thus the final topographic point clouds, revealed that there were numerous points shared across the survey years (Figure 5). For example, over 10,000 tie points were generated from the 2002 photos, and 337 of these were shared with the 2004 photos (Figure 5). In general, shared tie points were most numerous for surveys closest in time and for surveys for which the topographic change between surveys was minimal, such as between 2008 and 2009. These shared tie points provided geometric linkages between the photos of all surveys and are a primary factor for the low uncertainties reported below.

Uncertainty of SfM Point Clouds

Comparisons of SfM point clouds and LIDAR data were used to assess the quality of the SfM products and the amount and distribution of ground control points required for the analyses. Over the entire study area, the mean differences between the 2010 SfM and the 2010 LIDAR data were less than 0.1 m for all runs with ground control points (Figure 6a). The RSME and the irreducible error (calculated as the square root of the difference between the squared RMSE and the squared mean error) generally decreased with the number of ground control points (Figures 6b and c); however, the reduction in these errors was greatest between 3 and 12 ground points, and these errors were somewhat constant at ~0.2 m with 15 or more ground control points (Figures 6b and c). Limiting the ground control points to only those at the top of the cliff resulted in somewhat lower mean errors but higher RMS and irreducible errors (Figure 6).

Three-dimensional maps of the differences between the SfM- and LIDAR-derived point clouds provide spatial context to these errors (Figure 7). For example, with only three ground control points, the differences between the SfM and LIDAR data approached 0.5 m for a broad section of the study-area cliff face and exceeded 1.0 m on the study area's southern end (Figure 7a). Differences between the SfM and LIDAR data were negligible, however, in areas within ~10 m of the ground control point locations (Figure 7a).

Adding more ground control points reduced the differences between the SfM and LIDAR data, as shown with examples with 6 and 25 ground control points (Figures 7b and c); however, because the distribution of ground control points was limited to the study area's buildings and structures, the 41 usable ground control points were clustered in groups around these structures (*e.g.*, see the 25 points shown in Figure 7c). Although differences between SfM and LIDAR data were negligible near these clusters of points, deviations were greatest in areas far from the clusters such as on the northern section of the cliff face in the 25-ground control point example (Figure 7c).

These effects can be observed in an along-cliff synthesis of the SfM-LIDAR differences for these three models (Figure 8). The magnitude of error clearly decreases from three to six ground control points, but spatial patterns of errors become more irregular from 6 to 25 ground control points. Thus, although the bulk RMSE metrics for the 6 and 25 ground control point models were similar at 0.180 and 0.183 m, respectively, the spatial patterns of these errors were less irregular—and hence more preferred—for the six ground control point model. This suggests that there is likely an optimal range in number and distribution of ground control points for a study site and that for the Fort Funston area studied here, six well-distributed points achieved these preferred results.

Hence, for the remaining presentation of SfM results in this paper, topographic point clouds will be presented from analyses derived from six ground control points. Although six ground control points provided good comparative results for the 2010 photographic survey (RMSE = 0.180 m), no quantitative ways occurred to assess the accuracy of the remaining four surveys with these six points. Because of the similar setup and analyses, it was assumed that the accuracies of the remaining SfM-derived point clouds were generally similar to the distribution of errors shown in Figure 6. This would suggest 0.2 to 0.3 m of uncertainty in the 2002–09 point clouds if six ground control points were used. Thus, the total change-detection uncertainties are approximated to be ±0.5 m, which conservatively assumes that systematic biases may exist.
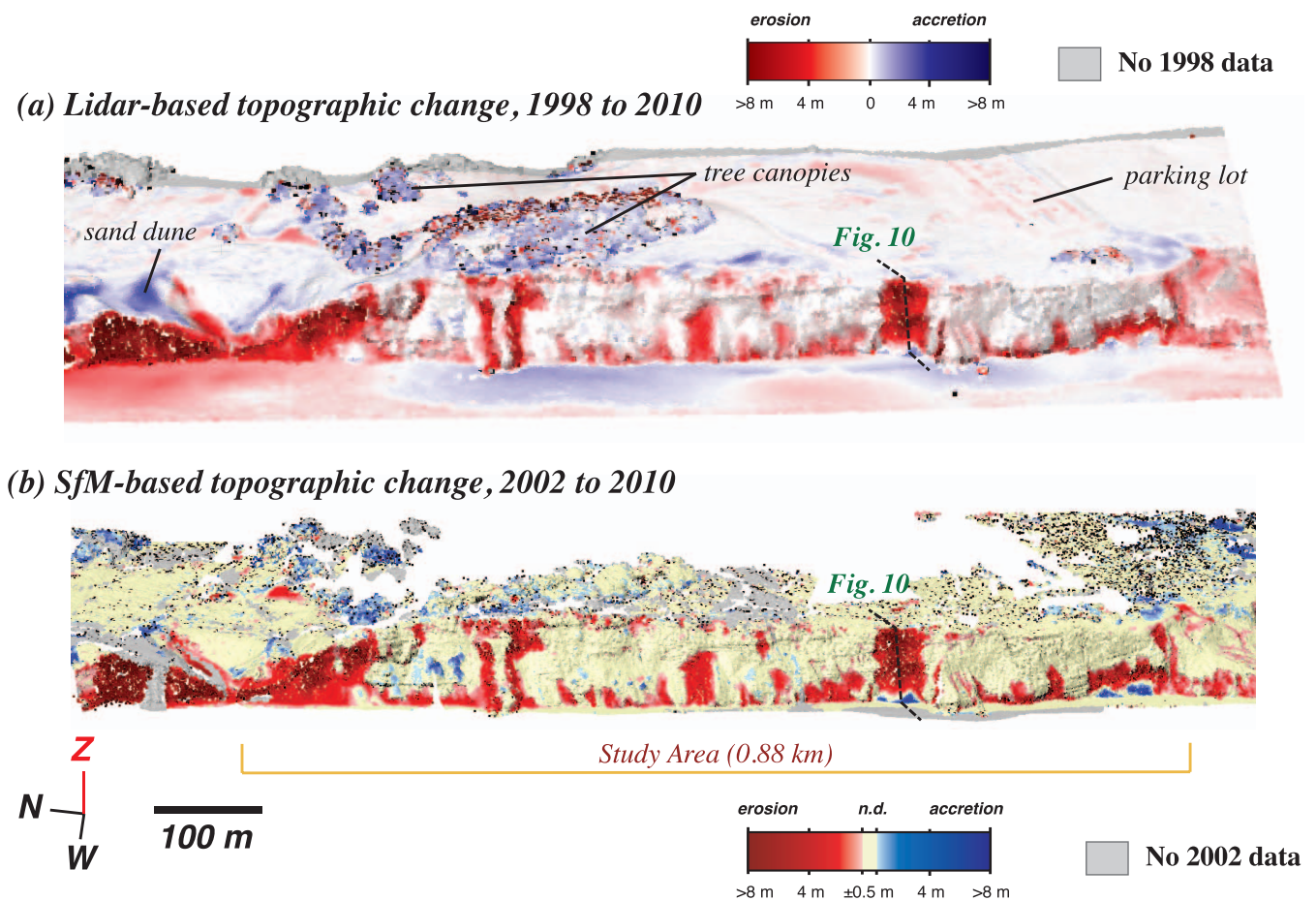
Figure 9. Comparison of difference maps for the Fort Funston study area derived from (a) 1998–2010 airborne LIDAR and (b) 2002–10 SfM topographic point clouds. Maps shown from oblique perspectives.

Comparison of SfM- and LIDAR-Measured Topographic Changes

The spatial patterns of topographic change measured independently from LIDAR and SfM were similar in pattern and scale (Figure 9). Although the difference in temporal resolution of these data (1998–2010 *vs.* 2002–10) limits direct comparisons, spatial similarities in change provides evidence that most of the changes observed in the 1998–2010 LIDAR data occurred during 2002–10. The SfM provided finer resolution observations of topographic change on the cliff face, however, owing to the one to two order-of-magnitude higher data densities and the oblique perspectives of the photographs (Figure 9). Although SfM provided higher resolution measurements of change on the cliff face, it provided inadequate measurements of change on the cliff top, where the LIDAR measurements revealed changes to the sand dunes, differences in the tree canopies, and changes in the distribution of automobiles in the parking lot (Figure 9a).

Profiles of the LIDAR and SfM data revealed strong similarities, such as shown for the largest landslide observed in the data (Figure 10). In this example, both datasets suggested that the upper 40 m of the cliff retreated ~12 m
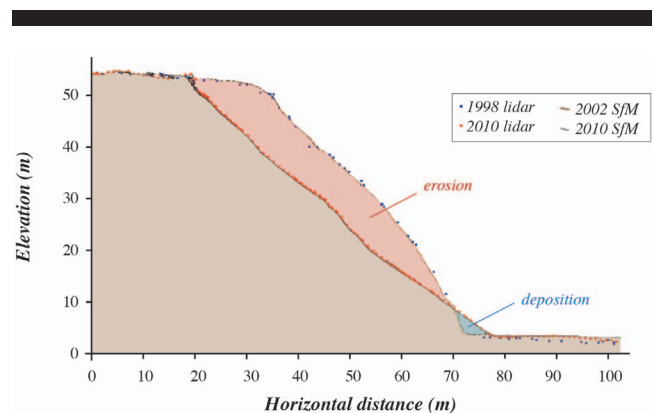

Figure 10. Comparison of LIDAR and SfM data across a cliff profile through the largest landslide observed in the data. Location of the profile identified in Figure 9. Shading added to highlight the SfM results and the erosion and deposition inferred from these data. (Color for this figure is available in the online version of this paper.)
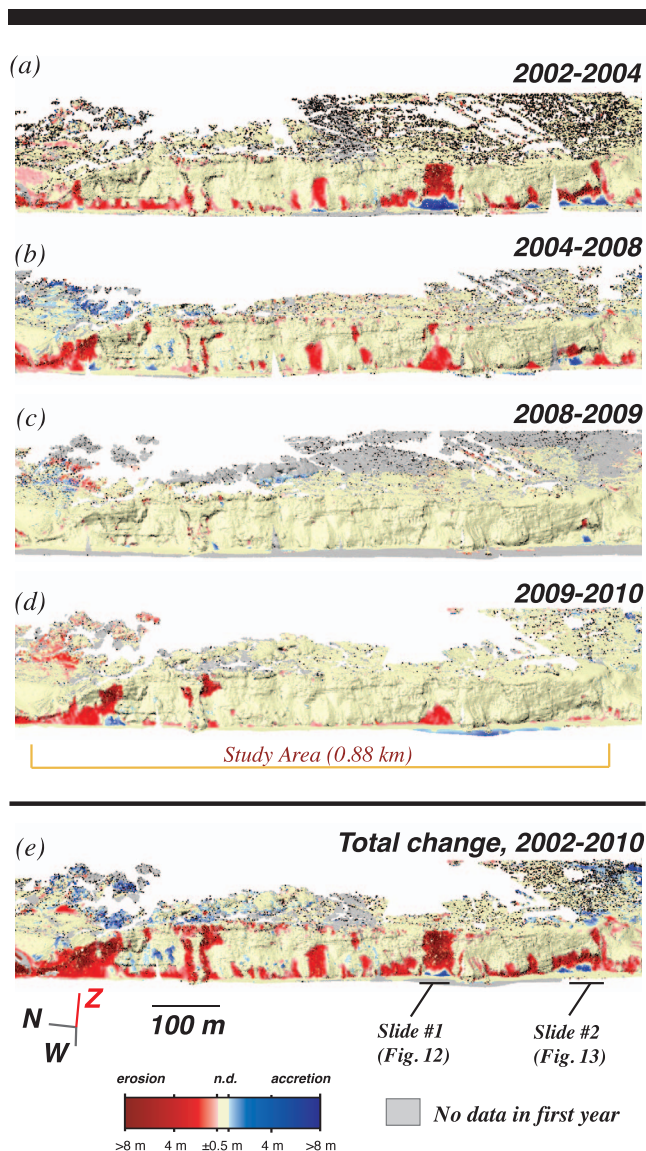
Figure 11. Three-dimensional difference maps between 2002 and 2010 for the Fort Funston study area using SfM developed with six ground control points. Yellow areas have differences less than the overall change detection uncertainty of ±0.5 m. Grey areas do not have data in the first of the two differenced point clouds. Difference maps are presented in the direction normal to the SfM-generated surface using the M3C2 methods of Lague, Brodu, and Leroux (2013). Change maps include (a) 2002–04, (b) 2004–08, (c) 2008–09, (d) 2009–10, and (e) the total change occurring during 2002–10.

landward. Furthermore, strong similarities are observed in the topography of the earliest data, the 1998 LIDAR and the 2002 SfM (Figure 10). This observation is supported by a comparison of data for a 70-m alongshore section adjacent to this profile that had no apparent rock falls or landslides between 1998 and 2002, for which a mean difference of 0.127 m and a RMSE of 0.296 m were measured (M3C2 difference metric; data not shown). These uncertainty levels are consistent with the error analysis of the 2010 LIDAR and SfM data reported previously. Yet, the data density of the 1998 LIDAR (~3 m nominal spacing on a horizontal plane) produced sizable data gaps in the

steepest portions of the landscape, such as observed near the base of the cliff (Figure 10). Gaps such as these will result in an underestimation of talus deposition from LIDAR data profiles, such as that shown in Figure 10.

Fort Funston Changes Observed with SfM

A compilation of the five SfM surveys reveals a time history of erosional patterns along the Fort Funston cliff (Figure 11). The most widespread erosion occurred during the first interval of time, 2002–04, during which multiple landslides were observed, most of which resulted in 2 to 12 m of erosion perpendicular to the cliff and centered predominantly on the lower half of the cliff face (Figure 11a). During this interval of time, many of the slides in the central to southern portions of the study area resulted in talus deposition on the beach, whereas deposition was not observed in the northern portion of the study area (Figure 11a). Erosional activity was reduced during the next three intervals of time spanning 2004–10 (Figures 11b–d). In fact, little change occurred during the 2008–09 interval except for some small (less than 10 m wide) rock falls (Figure 11c).

A more detailed presentation of two of the larger landslides—Slides #1 and #2 in Figure 11—demonstrates different erosional patterns (Figures 12 and 13). The largest slide, Slide #1, failed during the 2002–04 interval and resulted in over 12 m of landward movement of the cliff top and talus deposition over the lower portion of the cliff (Figure 12). This represented approximately 10,000 m^3 of erosion and 3400 m^3 of deposition for a net change of 6600 m^3. A profile through this slide from the SfM data clearly reveals these patterns of erosion and deposition (Figure 14a). During the subsequent four years (2004–08), erosion occurred in the landslide talus and along the headwall and northern sidewall of the landslide scarp (Figures 12 and 14a). Negligible change occurred during 2008–09, as shown by the topographic point clouds and the patterns of vegetation reestablishment observed in the photographs (Figure 12). Finally, roughly 3 m of landward erosion of the talus occurred during 2009–10 (Figure 14a), which coincided with ~1 m of undercutting of the cliff base north of the slide (Figure 12). In total, the landslide resulted in 12,200 m^3 of net erosion between 2002 and 2010.

The patterns of change at Slide #2 were also initiated with landslides during 2002–04, although in contrast with Slide #1 most of the failure occurred in the bottom half of the cliff with one ~10-m-wide erosional section extending up to the cliff top (Figure 13). Subsequent changes in this region during 2004–10 included erosion of the talus and failures at the top of the previous headwall in 5–10 m vertical sections of the cliff (Figure 13). When observed in profile, this resulted in complex changes that included headwall erosion and variations in the size and extent of talus on the beach (Figure 14b). Importantly, the SfM data adequately characterized these changes over a ~6-m-high section of the cliff topography that was overhanging past vertical (Figure 14b).

DISCUSSION

Changes to coastal cliffs are inherently complex because of the stochastic nature of erosion in time and a diversity of physical processes that act upon and may be responsible for
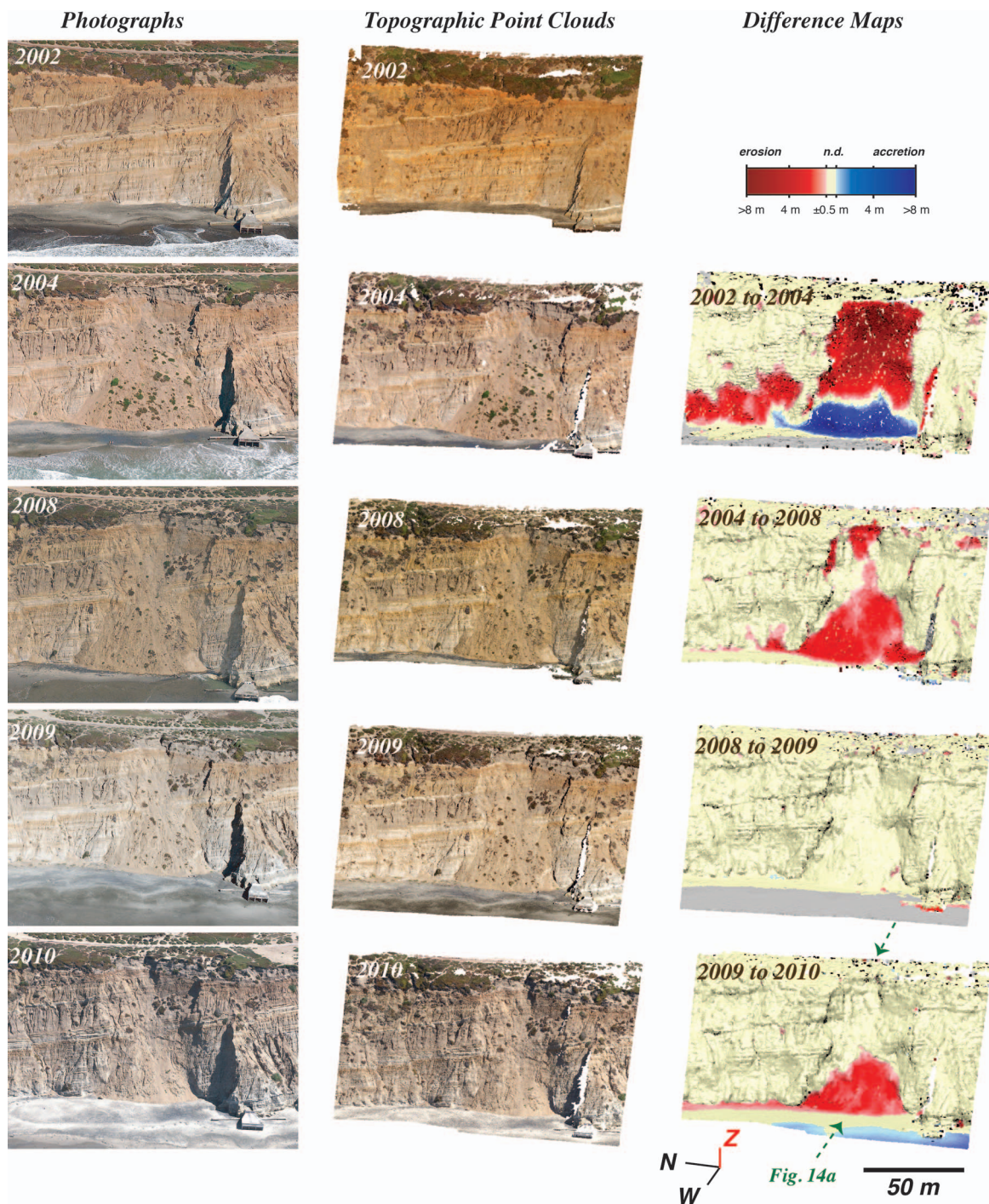
Figure 12. Topographic changes measured with SfM for the largest landslide that was measured at the Fort Funston study area (Slide #1 in Figure 11e). Included are original CCRP (2016) photographs (left column), topographic point clouds from the SfM analyses (central column), and the difference maps between subsequent point clouds (right column). Yellow areas have differences less than the local change detection uncertainty of ±0.5 m.

these changes (Emery and Kuhn, 1982; Hall *et al.*, 2002; Hapke, Reid, and Richmond, 2009; Rosser *et al.*, 2013; Sunamura, 1992; Trenhaile, 1987; Young *et al.*, 2011). Topographic data are essential because they reveal patterns of cliff failure, talus erosion, and beach change, which can be used, in turn, to better understand the processes responsible for erosion of sea cliffs (*e.g.*, Collins and Sitar, 2008; Hampton, 2002; Vann Jones *et al.*, 2015; Young, 2015; Young *et al.*, 2009).
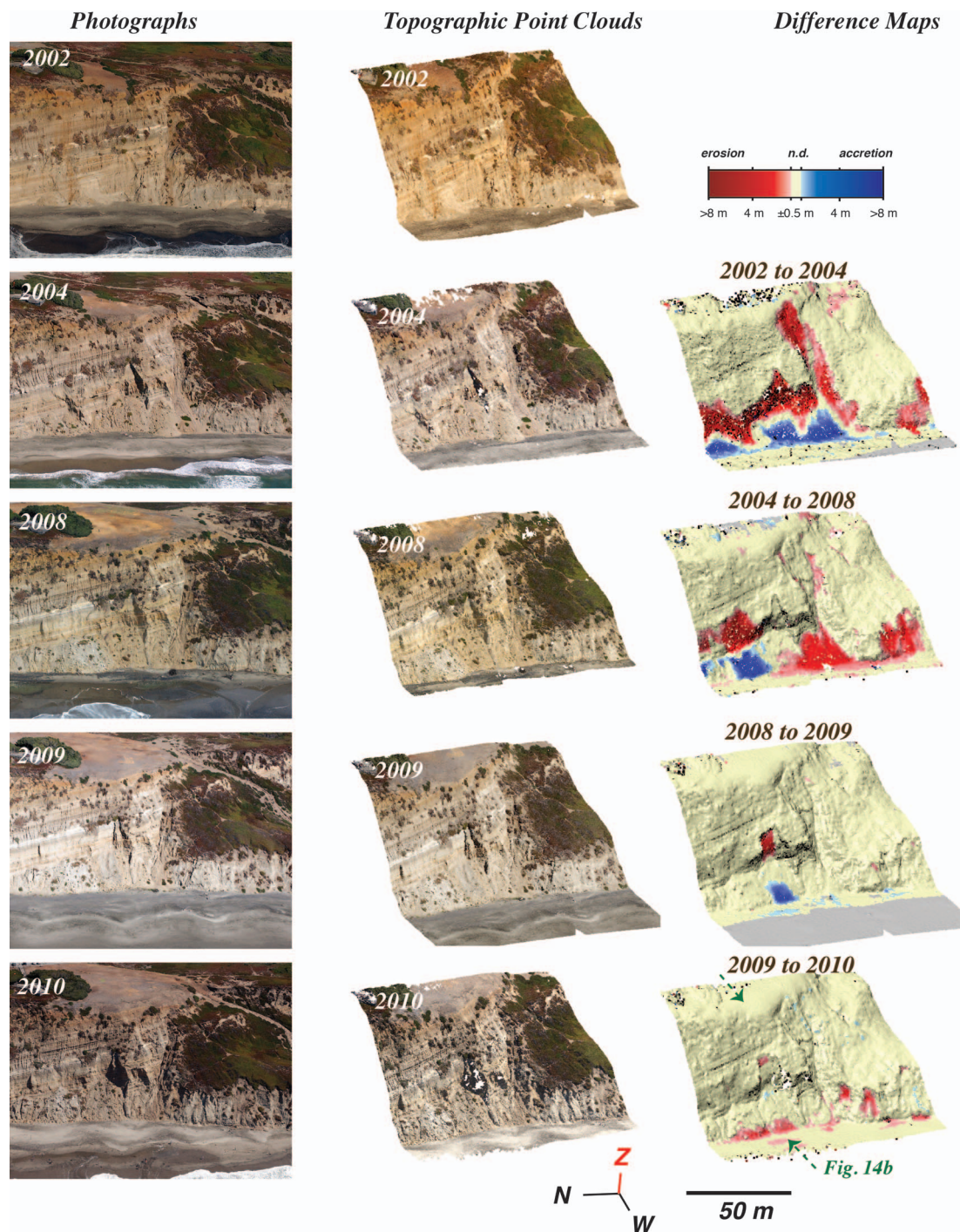
Figure 13. Topographic changes measured with SfM for a landslide complex at the Fort Funston study area (Slide #2 in Figure 11e). Included are original CCRP (2016) photographs (left column), topographic point clouds from the SfM analyses (central column), and the difference maps between subsequent point clouds (right column). Yellow areas have differences less than the local change detection uncertainty of ±0.5 m.

Topographic measurements and the understanding gained from them are necessary for predicting the future response of coastal cliffs to storms and sea-level rise (Bray and Hooke, 1997; FitzGerald *et al.*, 2008; Hapke and Plant, 2010; Limber

and Murray, 2011; Trenhaile, 2011; Walkden and Hall, 2005; Young *et al.*, 2014).

In this context, the new SfM techniques reported herein should provide necessary contributions toward new under-
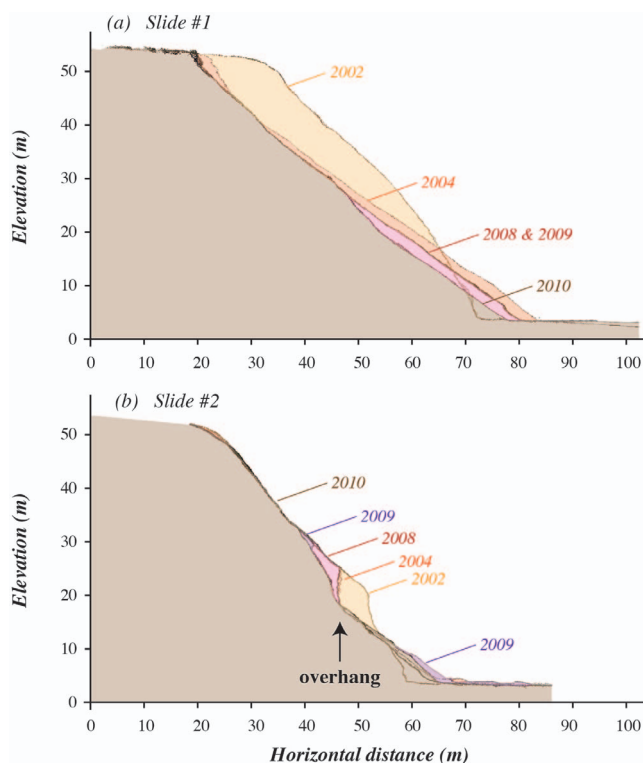
Figure 14. Profiles of the topographic changes during 2002–10 measured with SfM for two landslides of the Fort Funston study area: (a) Slide #1 and (b) Slide #2. Dates of the profile lines are highlighted with text and shading, and locations of profiles are shown in Figures 12 and 13. A region of overhang is shown in (b). (Color for this figure is available in the online version of this paper.)

standing and predictive efforts of sea-cliff change by providing high-resolution data in space and time to test model assumptions and confirm results. Compared with airborne LIDAR, the SfM techniques resulted in many-fold higher data densities (Table 2) with roughly the same data uncertainties. Thus, high potential exists for these SfM techniques to fill time-series gaps in topographic data for coasts around the world. This is attributable to the somewhat common occurrence of oblique photographic surveys along coasts compared to the availability of LIDAR. One exception is the southern California region where numerous airborne and ground-based LIDAR surveys have been conducted (Young, 2015; Young *et al.*, 2011).

An additional benefit of SfM from oblique photos is the dense topographic point clouds derived on vertical-to-overhanging landscapes (Figure 14), which are locations that airborne LIDAR generally do not image well (Gienko and Terry, 2014; Ružić *et al.*, 2014). Furthermore, investigations using oblique photographs will benefit from the information—such as vegetation patterns and cliff conditions—that can be interpreted from the raw photos and the inherited RGB-color values in the point clouds (*e.g.*, Figures 12 and 13).

Hence, it is concluded that oblique photos of coastal landforms have additional utility in the mapping of coastal topography and change. To realize these utilities, the photos

must have adequate overlap and some ground control and/or camera position information. A minimum photographic overlap threshold is that every point on the landscape must be observed in at least two photos. Examination of other imagery in the CCRP (2016) suggests that this requirement is regularly achieved along the state of California, and as such our techniques appear to be applicable to California's entire coastline. Other coastal photographic surveys, such as the Washington State Coastal Atlas (2016), while providing imagery for long, continuous sections of shoreline, do not appear to meet these basic overlap requirements and would not likely work adequately with SfM. Further testing and use of historical photographs worldwide is encouraged, as these records may provide vital information on past coastal topographies (*cf.* Derrien *et al.*, 2015; Gomez, Hayakawa, and Obanawa, 2015).

One important consideration for these future assessments is the use of the 4D photo alignment techniques described in the Method section. Point clouds generated using these techniques are enhanced by the tie points that connect across survey dates (*e.g.*, Thieler and Danforth, 1994). Although these across-survey tie points were few (less than 10% of the total number of the tie points for any annual survey in our study; Figure 5), they provided thousands of geometrical links across the study area and across multiple survey dates and were important, therefore, to the precision of the final alignment of the SfM point clouds.

Expanding these techniques to sections of coast longer than the 0.88 km studied here will not require significant changes in overall strategy; however, careful considerations will be needed to assess the number and density of ground control points necessary for larger or more complex areas. Additionally, longer sections of coast will require the facilitation of larger data sets than those developed here (*cf.* Table 2). This may require enhanced computing and data-storage resources, staged data-processing routines, or data-reduction strategies such as point cloud subsampling employed previously.

Future applications may also address locations where it is not feasible to incorporate survey-grade ground control points. In such cases, it may be adequate to use ground control points that are identifiable within the photos across multiple surveys that can be assumed to be stationary in space but do not have position information. Or, it may be adequate to incorporate ground control positions that are estimated from data such as airborne LIDAR. These types of ground control points, along with position information saved with each photo, may provide links to ensure adequate precision in the final point clouds and, hence, adequate assessments of topographic change, even though the final point clouds may not be adequately registered to true coordinates. That is, future efforts may find that SfM point clouds may be generated with adequate scaling but without accurate geopositioning for areas without survey-grade ground control points. Preliminary analyses with these techniques have been successful, but a thorough analysis is still outstanding and beyond the scope of this paper.

CONCLUSIONS

An investigation of historical oblique photographs of the California coast revealed that accurate and precise maps of

topography and topographic change could be developed using SfM and a select number of ground control points. Detailed descriptions of these techniques were provided, which should ease the transferability of the SfM techniques to other sites. This suggests that imagery that was originally obtained to provide qualitative assessments of shoreline change and coastal development may be used in quantitative assessments of topography and topographic change. The techniques reported here might be broadly applicable to photograph collections of coasts throughout the world, and further application and testing of these techniques is encouraged.

ACKNOWLEDGMENTS

LITERATURE CITED

Adams, J. and Chandler, J., 2002. Evaluation of LIDAR and medium scale photogrammetry for detecting soft-cliff coastal change. *The Photogrammetric Record*, 17(99), 405–418.

Agisoft, 2014. *Agisoft PhotoScan User Manual, Profession Edition*. Version 1.1, St. Petersburg, Russia: Agisoft, LLC, 66p.

Agisoft PhotoScan Pro software, version 1.1.6, 2016. http://agisoft-photoscan-professional.software.informer.com/download/.

Barnard, P.L.; Hansen, J.E., and Erikson, L.H., 2012. Synthesis study of an erosion hot spot, Ocean Beach, California. *Journal of Coastal Research*, 28(4), 903–922.

Bird, E.C.F., 1985. *Coastline Changes: A Global Review*. New York: John Wiley and Sons, 219p.

Bray, M.J. and Hooke, J.M., 1997. Prediction of soft-cliff retreat with accelerating sea-level rise. *Journal of Coastal Research*, 13(2), 453–467.

California Coastal Records Project (CCRP), 2016. http://www.californiacoastline.org/.

Cazenave, A. and Cozannet, G.L., 2014. Sea level rise and its coastal impacts. *Earth's Future*, 2(2), 15–34.

Clifton, H.E. and Hunter, R.E., 1999. Depositional and other features of the Merced Formation in seacliff exposures south of San Francisco, California. *In:* Wagner, D.L. and Graham, S.A. (eds.), *Geologic Field Trips in Northern California: California Division of Mines and Geology Special Publication 119*, pp. 89–100.

Cloud Compare software, version 2.6.1, 2016. http://cloudcompare.software.informer.com/2.6/.

Collins, B.D. and Sitar, N., 2008. Processes of coastal bluff erosion in weakly lithified sands, Pacifica, California, USA. *Geomorphology*, 97(3), 483–501.

Cowell, P.J. and Kench, P.S., 2001. The morphological response of atoll islands to sea-level rise. Part 1: Modifications to the shoreline translation model. *In:* Cooper, J.A.G. and Jackson, D.W.T. (eds.), *ICS 2000 Proceedings. Journal of Coastal Research*, Special Issue No. 34, pp. 633–644.

Crowell, M.; Leatherman, S.P., and Buckley, M.K., 1991. Historical shoreline change: Error analysis and mapping accuracy. *Journal of Coastal Research,* 7(3), 839–852.

Derrien, A.; Villeneuve, N.; Peltier, A., and Beauducel, F., 2015. Retrieving 65 years of volcano summit deformation from multi-temporal Structure-from-Motion: The case of Piton de la Fournaise (La Réunion Island). *Geophysical Research Letters*, 42(17), 6959–6966.

Eltner, A.; Baumgart, P.; Maas, H.G., and Faust, D., 2015. Multi-temporal UAV data for automatic measurement of rill and interrill erosion on loess soil. *Earth Surface Processes and Landforms*, 40(6), 741–755.

Emery, K.O. and Kuhn, G.G., 1982. Sea cliffs: Their processes, profiles, and classification. *Geological Society of America, Bulletin*, 93(7), 644–654.

Fitzgerald, D.M.; Fenster, M.S.; Argow, B.A., and Buynevich, I.V., 2008. Coastal impacts due to sea-level rise. *Annual Reviews of Earth and Planetary Sciences*, 36, 601–647.

Fletcher, C.; Rooney, J.; Barbee, M.; Lim, S.C., and Richmond, B., 2003. Mapping shoreline change using digital orthophotogrammetry on Maui, Hawaii. *In:* Byrnes, M.R.; Crowell, M., and Fowler, C. (eds.), *Shoreline Mapping and Change Analysis: Technical Considerations & Management Implications. Journal of Coastal Research*, Special Issue No. 38, pp. 106–124.

Fonstad, M.A.; Dietrich, J.T.; Courville, B.C.; Jensen, J.L., and Carbonneau, P.E., 2013. Topographic structure from motion: A new development in photogrammetric measurement. *Earth Surface Processes and Landforms*, 38(4), 421–430.

Gienko, G.A. and Terry, J.P., 2014. Three-dimensional modeling of coastal boulders using multi-view image measurements. *Earth Surface Processes and Landforms*, 39(7), 853–864.

Gomez, C.; Hayakawa, Y., and Obanawa H., 2015. A study of Japanese landscapes using structure from motion derived DSMs and DEMs based on historical aerial photographs: New opportunities for vegetation monitoring and diachronic geomorphology. *Geomorphology*, 242, 11–20. doi:10.1016/j.geomorph.2015.02.021

Google Earth, 2016. http://www.google.com/earth/.

Hall, J.W.; Meadowcroft, I.C.; Lee, E.M., and van Gelder, P.H.A.J.M., 2002. Stocastic simulation of episodic soft coastal cliff recession. *Coastal Engineering*, 46(3), 159–174.

Hampton, M., 2002. Gravitational failure of sea cliffs in weakly lithified sediment. *Environmental and Engineering Geoscience*, 8(3), 175–191.

Hapke, C.J. and Plant, N., 2010. Predicting coastal cliff erosion using a Bayesian probabilistic model. *Marine Geology,* 278(1), 140–149.

Hapke, C.J. and Reid, D., 2007. National Assessment of Shoreline Change Part 4: Historical Coastal Cliff Retreat along the California Coast. *U.S. Geological Survey Open-File Report 2007-1133*, 51p.

Hapke, C.J. and Richmond, B., 2000. Monitoring beach morphology changes using small-format aerial photography and digital softcopy photogrammetry. *Environmental Geosciences*, 7(1), 32–37.

Hapke, C.J.; Reid, D., and Richmond, B., 2009. Rates and trends of coastal change in California and the regional behavior of the beach and cliff system. *Journal of Coastal Research*, 25(3), 603–615.

James, M.R. and Robson, S., 2012. Straightforward reconstruction of 3D surfaces and topography with a camera: Accuracy and geoscience application. *Journal of Geophysical Research: Earth Surface*, 117, F03017. doi:10.1029/2011JF002289

James, M.R. and Robson, S., 2014. Mitigating systematic error in topographic models derived from UAV and ground-based image networks. *Earth Surface Processes and Landforms*, 39(10), 1413–1420.

Javernick, L.; Brasington, J., and Caruso, B., 2014. Modeling the topography of shallow braided rivers using Structure-from-Motion photogrammetry. *Geomorphology*, 213, 166–182. doi:10.1016/j.geomorph.2014.01.006

Johnson, K.; Nissen, E.; Saripalli, S.; Arrowsmith, J.R.; McGarey, P.; Scharer, K.; Williams, P., and Blisniuk, K., 2014. Rapid mapping of ultrafine fault zone topography with structure from motion. *Geosphere*, 10(5), 969–986.

Lague, D.; Brodu, N., and Leroux, J., 2013. Accurate 3D comparison of complex topography with terrestrial laser scanner: Application to the Rangitikei canyon (NZ). *ISPRS Journal of Photogrammetry and Remote Sensing*, 82, 10–26.

Larson, M. and Kraus, N.C., 1994. Temporal and spatial scales of beach profile change, Duck, North Carolina. *Marine Geology*, 117(1), 75–94.

Limber, P.W. and Murray, A.B., 2011. Beach and sea-cliff dynamics as a driver of long-term rocky coastline evolution and stability. *Geology*, 39(12), 1147–1150.

Limber, P.W.; Patsch, K.B., and Griggs, G.B., 2008. Coastal sediment budgets and the littoral cutoff diameter: A grain size threshold for quantifying active sediment inputs. *Journal of Coastal Research*, 24(2A), 122–133.

McGranahan, G.; Balk, D., and Anderson, B., 2007. The rising tide: Assessing the risks of climate change and human settlements in low elevation coastal zones. *Environment and Urbanization*, 19(1), 17–37.

Micheletti, N.; Chandler, J.H., and Lane, S.N., 2015. Investigating the geomorphological potential of freely available and accessible structure-from-motion photogrammetry using a smartphone. *Earth Surface Processes and Landforms*, 40(4), 473–486.

Moore, L.J., 2000. Shoreline mapping techniques. *Journal of Coastal Research*, 16(1), 111–124.

Morgan, K.L.M. and Krohn, M.D., 2014. Post-Hurricane Sandy Coastal Oblique Aerial Photographs Collected from Cape Lookout, North Carolina, to Montauk, New York, November 4–6, 2012. *U.S. Geological Survey Data Series 858*. doi:10.3133/ds858

Morton, R.A.; Paine, J.G., and Gibeaut, J.C., 1994. Stages and durations of post-storm beach recovery, southeastern Texas coast, USA. *Journal of Coastal Research*, 10(4), 884–908.

National Oceanic and Atmospheric Administration (NOAA) Digital Coastal website, 2016. https://coast.noaa.gov/digitialcoast/.

Prosdocimi, M.; Calligaro, S.; Sofia, G.; Dalla Fontana, G., and Tarolli, P., 2015. Bank erosion in agricultural drainage networks: New challenges from structure-from-motion photogrammetry for post-event analysis. *Earth Surface Processes and Landforms*, 40(14), 1891–1906.

Randle, T.J.; bountry, J.A.; Ritchie, A., and Wille, K., 2015. Large-scale dam removal on the Elwha River Washington USA: Erosion of reservoir sediment. *Geomorphology*, 246, 709–728.

Rosser, N.J.; Brain, M.J.; Petley, D.N.; Lim, M., and Norman, E.C., 2013. Coastline retreat via progressive failure of rocky coastal cliffs. *Geology*, 41(9), 939–942.

Ruggiero, P.; Kaminsky, G.M.; Gelfenbaum, G., and Voigt, B., 2005. Seasonal to interannual morphodynamics along a high-energy dissipative littoral cell. *Journal of Coastal Research*, 17(2), 553–578.

Ruggiero, P.; Komar, P.D.; McDougal, W.G.; Marra, J.J., and Beach, R.A., 2001. Wave runup, extreme water levels and the erosion of properties backing beaches. *Journal of Coastal Research*, 17(2), 407–419.

Ruggerio, P.; Kratzmann, M.G.; Himmelstoss, E.A.; Reid, D.; Allan, J., and Kaminsky, G., 2013. National Assessment of Shoreline Change: Historical Shoreline Change along the Pacific Northwest Coast. *U.S. Geological Survey Open-File Report 2012-1007*, 62p.

Ružić, I.; Marović, I.; Benac, Č., and Ilić, S., 2014. Coastal cliff geometry derived from structure-from-motion photogrammetry at Stara Baška, Krk Island, Croatia. *Geo-Marine Letters*, 34(6), 555–565.

Ryan, H.F.; Parsons, T., and Sliter, R.W., 2008, Vertical tectonic deformation associated with the San Andreas Fault zone offshore of San Francisco, California. *Tectonophysics*, 457(3), 209–223.

Sallenger, A.H.; Krabill, W.; Brock, J.; Swift, R.; Manizade, S., and Stockdon, H., 2002. Sea-cliff erosion as a function of beach changes and extreme wave runup during the 1997–1998 El Niño. *Marine Geology*, 187(3), 279–297.

Smith, G.L. and Zarillo, G.A., 1990. Calculating long-term shoreline recession rates using aerial photographic and beach profiling techniques. *Journal of Coastal Research*, 6(1), 111–120.

Snavely, N.; Seitz, S.M., and Szeliski, R., 2006. Photo tourism: Exploring photo collections in 3D. *ACM Transactions on Graphics*, 25(3), 835–846.

Stockdon, H.F.; Sallenger, Jr., A.H.; List, J.H., and Holman, R.A., 2002. Estimation of shoreline position and change using airborne topographic lidar data. *Journal of Coastal Research*, 18(3), 502–513.

Sunamura, T., 1992. *Geomorphology of Rocky Coasts*. Hoboken, NJ: John Wiley, 302p.

Thieler, E.R. and Danforth, W.W., 1994. Historical shoreline mapping (I): Improving techniques and reducing positioning errors. *Journal of Coastal Research*, 10(3), 549–563.

Trenhaile, A.S., 1987. *The Geomorphology of Rock Coasts*. Oxford, U.K.: Oxford University Press, 384p.

Trenhaile, A.S., 2011. Predicting the response of hard and soft rock coasts to changes in sea level and wave height. *Climate Change*, 109(3), 599–615.

Vann Jones, E.C. (née Norman); Rosser N.J.; Brain, M.J., and Petley, D.N., 2015. Quantifying the environmental controls on erosion of a hard rock cliff. *Marine Geology*, 363, 230–242.

Walkden, M.J.A. and Hall, J.W., 2005. A predictive mesoscale model of the erosion and profile development of soft rick shores. *Coastal Engineering*, 52(6), 535–563.

Washington State Coastal Atlas, 2016. https://fortress.wa.gov/ecy/coastalatlas/.

Westoby, M.J.; Brasington, J.; Glasser, N.F.; Hambrey, M.J., and Reynolds, J.M., 2012. 'Structure-from-Motion' photogrammetry: A low-cost, effective tool for geoscience applications. *Geomorphology*, 179, 300–314.

White, K. and El Asmar, H.M., 1999. Monitoring changing position of coastlines using Thematic Mapper imagery, an example from the Nile Delta. *Geomorphology*, 29(1), 93–105.

Young, A.P., 2015. Recent deep-seated coastal landsliding at San Onofre State Beach, California. *Geomorphology*, 228, 200–212.

Young, A.P.; Flick, R.E.; O'Reilly, W.C.; Chadwick, D.B.; Crampton, W.C., and Helly, J.J., 2014. Estimating cliff retreat in southern California considering sea level rise using a sand balance approach. *Marine Geology*, 348, 15–26.

Young, A.P.; Guza, R.T.; Flick, R.E.; O'Reilly, W.C., and Gutierrez, R., 2009. Rain, waves, and short-term evolution of composite seacliffs in southern California, *Marine Geology*, 267(1–2), 1–7.

Young, A.P.; Guza, R.T.; O'Reilly, W.C.; Flick, R.E., and Guitierrez, R., 2011. Short-term retreat statistics of a slowly eroding coastal cliff. *Natural Hazards and Earth System Science,* 11(1), 205–217.

Young, A.P.; Olsen, M.J.; Driscoll, N.; Flick, R.E.; Gutierrez, R.; Guza, R.T.; Johnstone, E., and Kuester, F., 2010. Comparison of airborne and terrestrial lidar estimates of seacliff erosion in southern California. *Photogrammetric Engineering and Remote Sensing*, 76(4), 421–427.